© Indian Academy of Sciences

SCIENCE RESULTS

UOCS. IV. Discovery of diverse hot companions to blue stragglers in the old open cluster King 2

VIKRANT V. JADHAV[1,2,*] (iD), SINDHU PANDEY[3] (iD), ANNAPURNI SUBRAMANIAM[1] and RAM SAGAR[1,3]

[1] Indian Institute of Astrophysics, Sarjapur Road, Koramangala, Bangalore 560 034, India.
[2] Joint Astronomy Programme and Department of Physics, Indian Institute of Science, Bangalore 560 012, India.
[3] Aryabhatta Research Institute of Observational Sciences, Manora Peak, Nainital 263 002, India.
*Correspondence author. E-mail: vikrant.jadhav@iiap.res.in

Abstract. King 2, one of the oldest clusters in the Milky Way, with an age of ~ 6 Gyr and distance of ~ 5700 pc, has been observed with UVIT payload on the AstroSat. With membership information derived from *Gaia* EDR3, the cluster is found to have 39 blue straggler stars (BSSs). We created multi-wavelength spectra-energy distributions (SED) of all the BSSs. Out of 10 UV detected BSSs, 6 bright ones were fitted with double component SEDs and were found to have hotter companions with properties similar to extreme horizontal branch (EHB)/subdwarf B (sdB) stars, with a range in luminosity and temperature, suggesting a diversity among the hot companions. We suggest that at least 15% of BSSs in this cluster are formed via mass-transfer pathway. When we compared their properties to EHBs and hotter companions to BSS in open and globular clusters, we suggest that EHB/sdBs like companions can form in binaries of open clusters as young as 6 Gyr.

1. Introduction

The evolution of binary systems strongly depends on the initial orbital parameters and its further evolution, where any change in their orbits can lead to a widely different evolution. If one of the stars evolves and fills its Roche lobe, the system will undergo mass transfer. Details such as duration and rate of mass transfer will depend on the orbits and masses of the binary stars. If such a binary is present in a star cluster, and the secondary of the binary has mass similar to the main sequence turnoff (MSTO) mass, then the secondary will become brighter than the MSTO and appear as a blue straggler star (BSS). Otherwise, the secondary will be fainter than the MSTO and can be classified as a blue lurker. The blue lurkers are identified by their high stellar rotation (Leiner *et al.* 2019) or evidence of extremely low-mass (ELM) white dwarf (WD) companion (Jadhav *et al.* 2019). Depending on the evolutionary status of binary components, the binary system can be observed as main sequence (MS)+MS, contact binaries (Rucinski 1998), common envelop, MS+horizontal branch (HB; Subramaniam *et al.* 2016), MS+extreme HB (EHB; Singh *et al.* 2020), MS+ subdwarf-B (sdB; Han *et al.* 2002), MS+WD (Jadhav *et al.* 2019), WD+WD (Marsh *et al.* 1995) and many more combinations. The binary evolution also depends on external factors such as collisions in a high-density environment which can decouple the binary (Heggie 1975) and

---

This article is part of the Special Issue on "AstroSat: Five Years in Orbit".

tertiary star which can expedite the mass transfer/ merger by reducing the orbital separation (Kozai 1962).

We are carrying out a long term project[1] of characterising products of binary stars such as BSSs in open clusters (OCs). Ultraviolet imaging of binary systems reveals the presence of hotter companions in the binary system, given that the hotter companion is luminous in UV. Old OCs such as NGC 188 and NGC 2682 are rich with BSSs, binary stars and contain many such optically sub-luminous UV-bright companions (Subramaniam *et al.* 2016; Sindhu *et al.* 2019; Jadhav *et al.* 2019). Similar companions have been identified to BSSs in the outskirts of GCs (Sahu *et al.* 2019; Singh *et al.* 2020). Subramaniam *et al.* (2020) provides a summary of the BSSs and post mass transfer systems in star clusters.

King 2 is one of the oldest clusters in the Milky Way, with an age of ~ 6 Gyr and distance of ~ 5700 pc (Table 1). However, it has been poorly studied due to its considerable distance and unknown membership information. For identifying and characterising hot BSSs and their possible companions, we obtained Ultra Violet Imaging Telescope (UVIT)/AstroSat observations of rich OC King 2 ($\alpha_{2000} = 12°.75$; $\delta_{2000} = +58°.183$; $l = 122°.9$ and $b = -4°.7$) under AstroSat proposal A02_170. Kaluzny (1989) presented the first optical colour-magnitude diagram (CMD) study of this distant cluster using *BV* CCD photometric data. This yielded a range of plausible ages and distances for different assumed reddenings and metallicities. The galactocentric distance of the cluster was estimated to be ~ 14 kpc. Aparicio *et al.* (1990) (A90 hereafter) did a comprehensive study on the cluster using *UBVR* photometry and derived an age of 6 Gyr and a distance of 5.7 kpc for solar metallicity. They also indicated the presence of a good fraction of binaries in the MS. Tadross (2001) estimated a value of [Fe/H] $= -0.32$ using the $(U - B)$ colour excess

from the literature data, while Warren and Cole (2009; WC09 hereafter) derived a value of [Fe/H] $= -0.42 \pm 0.09$ using spectroscopic data. These metallicity estimates are significantly sub-solar and inconsistent with the finding of A90. WC09 found a distance of 6.5 kpc and a slightly younger age, ~ 4 Gyr, better fitted the optical CMD and 2MASS Ks, red clump if the reddening is adopted as $E(B - V) = 0.31$ mag. This distance puts King 2 at RGC = 13 kpc, where its metallicity falls close to the trend of the galactic abundance gradients derived in Friel *et al.* (2002). There has been no proper motion study available for this cluster till *Gaia* DR2 (Gaia Collaboration *et al.* 2018). Cantat-Gaudin *et al.* (2018) provided a membership catalogue of King 2 with 128 members with *Gaia* DR2, and Jadhav *et al.* (2021) provided kinematic membership of 1072 stars (and 340 probable members) using kinematic data taken from *Gaia* EDR3.

Above discussed optical photometric studies indicate a good number of post-MS hot stars in King 2. In fact, Ahumada and Lapasset (2007) have identified 30 BSS candidates based on the location of these stars in the cluster. We present the UVIT and the archival data used in this study in the next section, followed by analyses, results and discussion.

2. UVIT and archival data

We observed King 2 with UVIT, which is one of the payloads on the first Indian multiwavelength space observatory AstroSat, launched on 28 September 2015. The observation was carried out by UVIT on 17 December 2016, simultaneously in two filters. The telescope has three channels with a set of filters in them: Far-UV (FUV; 130–180 nm), near-UV (NUV; 200–300 nm) and visible (VIS; 350–550 nm), where the VIS channel is intended to correct the drift of the

Table 1. Age, distance, reddening ($E(B - V)$) and metallicity of King 2 estimated by various investigators are listed.

Age (Gyr)	Distance (pc)	$E(B - V)$ (mag)	Metallicity	References
6.02	5750	0.31	–0.42	Dias *et al.* (2002)
6	5690 ± 65	0.31 ± 0.02	–0.5 to –2.2	Aparicio *et al.* (1990)
			–0.32	Tadross (2001)
4 to 6	~ 7000	0.23 to 0.5		Kaluzny (1989)
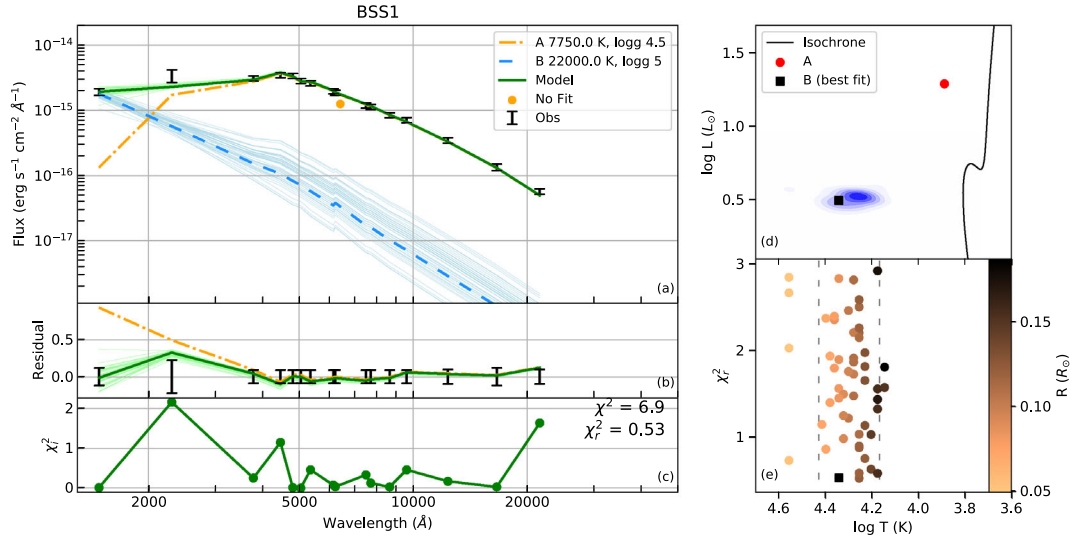
Figure 1. Two-component SED of BSS1. (**a**) Composite SED (green curve) is shown along with the observed flux (as black error-bars). The unfitted point (in this case: CAHA.R) is shown as orange dot. The cooler (BSS, orange dot-dashed curve) and hotter (blue dashed curve) component are also shown with their T_{eff} and $\log g$. The model, B component and residuals of noisy iterations are also shown as light coloured lines. (**b**) The fractional residual is shown for single component fit (orange dot-dashed curve) and composite fit (green solid curve). The fractional observational errors are also indicated on X-axis. (**c**) The χ_i^2 of each data point. (**d**) H–R diagram of the two components along with the isochrone for reference. The density distribution of the noisy B component fits is plotted in blue. (**e**) $T_{eff} - \chi^2$ distribution for the noisy B component fits coloured according to their radii. The dashed lines are the quoted limits of the temperature.

spacecraft (see Kumar *et al.* 2012; Tandon *et al.* 2017 for more details). The cluster was observed in one FUV (F148W, limiting magnitude ≈23 mag) and one NUV (N219M, limiting magnitude ≈22 mag) filter for exposure time of ∼2.7 ks. The FWHM of PSF in F148W and F219N images is 1″.33 and 1″.35 respectively. The data reduction was done using CCDLAB (Postma & Leahy 2017) and PSF photometry was performed using DAOPHOT package of IRAF (Tody 1993). More details of the reduction process are presented in Jadhav *et al.* (2021). We have detected ten member stars in either F148W and/or N219M filter.

We obtained archival optical (*UBVR*) photometry data from A90 catalogue (Calar Alto Observatory; CAHA) and cross-matched with UVIT data using TOPCAT (Taylor 2005). The cluster was observed with *GALEX* under All-sky Imaging Survey (AIS) in NUV filter (exp. time ∼100 s). All the detected member stars were further cross-matched with photometric data from UV to IR wavelength bands obtained from *GALEX* (Bianchi *et al.* 2000), PAN-STARRS PS1 (Chambers *et al.* 2016), *Gaia* EDR3 (Gaia Collaboration *et al.* 2020), 2MASS (Skrutskie *et al.* 2006), WISE (Wright *et al.* 2010) using virtual observatory tools in VOSA (Bayo *et al.* 2008).

3. SED fitting and colour magnitude diagrams

The data were corrected for reddening $(E(B - V) = 0.31 \pm 0.02)$ using Fitzpatrick (1999) and Indebetouw *et al.* (2005) and calibrated with the cluster distance of 5750±100 pc (we have overestimated the error to cover distance estimates from Dias *et al.* (2002) and A90). We have adopted the metallicity of [Fe/H]= −0.5 for all the stars and used Kurucz model spectrum (Castelli *et al.* 1997) for comparison. The SED fitting was done as follows:
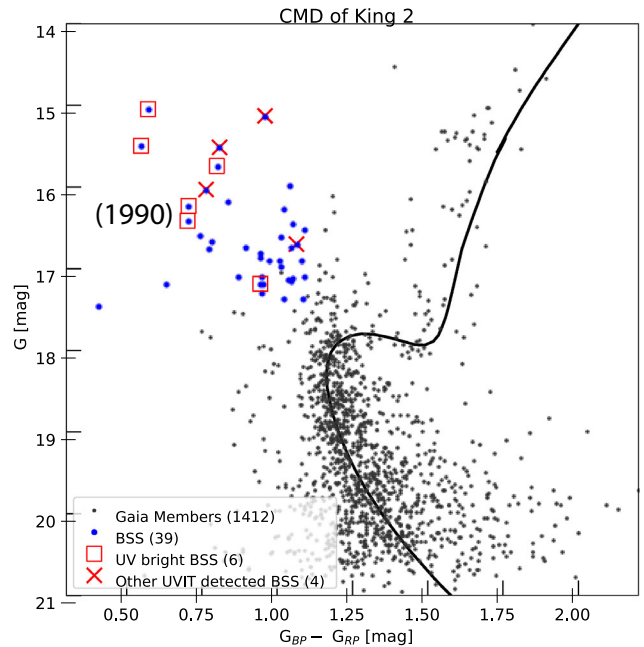
(1) We constructed the observed spectral energy distribution (SED) for all stars using the data from UV to IR wavelength, as mentioned above. The fluxes of all stars are given in Table 3.

(2) Kurucz models (Castelli *et al.* 1997) of $\log g \in (3.0, 5.0)$ were fitted to optical and IR points (above 3000 Å) using VOSA[2] (Bayo *et al.* 2008). There were some sources which showed UV excess in multiple UV points compared to the model fit. We selected such stars to be fitted with a two component SED. Otherwise, the single component fits are deemed satisfactory and are stated in the lower part of Table 2.

---

[2]http://svo2.cab.inta-csic.es/theory/vosa/index.php

(3) We used the cooler component parameters from above fits and then fitted a hotter component to the residual using `Binary_SED_Fitting`[3]. In preliminary double component fits, the hotter components were found to be compact objects, hence they were fitted with $\log g = 5$ Kurucz models.

(4) Very small errors in PAN-STARRS PS1, *Gaia* EDR3 and A90 photometry led to ignoring relatively high error UV data-points, hence they were replaced with mean errors for better residual across all wavelengths. A few data points were removed to achieve better fits and lower χ^2 (see Fig. 1(a)). The error values given in Table 3 are original unmodified errors. The detailed SED fitting method is explained in Section 3.3 of Jadhav *et al.* (2019).

(5) The best-fit parameters for single stars or cooler components are taken from the VOSA fits. The hotter component parameters are taken from the least χ^2 model in the two component fitting.

(6) The errors in cooler component parameters are fairly low and are taken as the grid values. To derive errors in the hotter component parameters, we used a statistical approach. We first generated 100 iterations of observed SEDs with added Gaussian noise in each data point. These 100 SEDs were then fitted with double components. However, not all the double fits converged, hence we only kept hotter components with $6000\,\mathrm{K} < T_{\mathrm{eff}} < 37000\,\mathrm{K}$. Logarithmic distributions of the parameters from the noisy and converging iterations were then fitted with Gaussian distributions. FWHM of these Gaussian distributions are defined as the upper and lower limits of the fitting parameters (temperature, radius and luminosity).

Figure 2 shows the CMD of 1412 cluster candidates identified from *Gaia* EDR3 with probability of over 50% (Jadhav *et al.* 2021) and are marked as grey points. Among these stars, we have selected 39 member stars brighter ($G < 17.5$ mag) and bluer ($G_{\mathrm{BP}} - G_{\mathrm{RP}} < 1.1$ mag) than the MSTO as BSSs. Seven of them were detected in F148W, and seven were detected in N219M (four in both filters). An isochrone of log age = 9.7 is over-plotted on the CMD. 20 of the BSSs are detected in the NUV filter of *GALEX*. We fitted Kurucz model SEDs to all BSSs and found excess UV flux in 15 BSS (BSS 1, 2, 3, 4, 5, 7, 8, 9, 10, 19, 26, 28, 29, 33 and 36). Among these,

Figure 2. CMD of King 2 cluster candidates using *Gaia* EDR3 data. All BSS members are shown as blue circles. The UV bright BSS (see Section 3) are shown as red squares, and other UVIT detected BSS are shown as red X's. The *Gaia* members are shown as black dots along with the PARSEC isochrone of log age = 9.7, [M/H] = –0.4, DM = 13.8 and $E(B - V) = 0.45$.

BSS1, 2, 3, 4, 5 and 7 have multiple UV data points from UVIT or *GALEX* or both. Only these six were fitted with double component SEDs, because a hot component fit can be reliable if the number of UV data points is more than one. Hereafter, these six BSS will be referred to as 'UV bright BSSs' and others will be referred to as 'UV faint BSSs'. The four BSS detected in UVIT but not fitted with hotter component are shown as red X's in the CMD.

We have shown an example of a double component SED fit of BSS1 in Fig. 1(a). The BSS1-A component is a BSS with 7750 K, while the BSS1-B component has T_{eff} of 22000 K. The reduction in residual after including the hotter component is visible in Fig. 1(b). The χ_i^2 for individual points is shown in Fig. 1(c) with χ_r^2 of 0.53. Although, we note that the χ_r^2 need not be ~ 1, for a non-linear model fitting (Andrae *et al.* 2010). One has to look at residuals and χ^2 both to determine the goodness of fit. Figure 1(d) shows the Hertzsprung–Russell (H–R) diagram of A and B components. The density distribution of noisy and converging iterations is also shown to get an idea of degeneracy in temperature and luminosity. Figure 1(e) panel shows the best fit and the noisy and converging

---

[3]https://github.com/jikrant3/Binary_SED_Fitting `Binary_SED_Fitting` is a python code which uses χ^2 minimisation technique to fit two component SEDs.

Table 2. Fitting parameters of the best fit of the double and single component fits of BSSs with the hotter component. Scaling factor is the value by which the model has to be multiplied to fit the data, N_{fit} is the number of data points fitted and χ_r^2 is the reduced χ^2 for the composite fit. The χ_r^2 values of single fits of the cooler components are given in brackets. Note: the $\log g$ values are imprecise due to the insensitivity of the SED to $\log g$.

Name	Comp.	$\log g$	T_{eff} [K]	R [$R_\odot$]	L [$L_\odot$]	Scaling factor	N_{fit}	χ_r^2 $(\chi_{r,\text{single}}^2)$
Double fits								
BSS1	A	4.5	7750 ± 125	2.44 ± 0.04	19.3 ± 1.8	8.99E-23	16	0.5 (10.5)
	B	5	$22000\,^{+4842}_{-7269}$	$0.122\,^{+0.150}_{-0.037}$	$3.1\,^{+0.7}_{-0.4}$	2.23E-25		
BSS2	A	3.5	8250 ± 125	3.72 ± 0.06	57.6 ± 3.4	2.09E-22	16	3.9 (1.2)
	B	5	$24000\,^{+6802}_{-4996}$	$0.234\,^{+0.131}_{-0.089}$	$16.4\,^{+1.5}_{-1.2}$	8.27E-25		
BSS3	A	4.5	7250 ± 125	3.56 ± 0.06	31.6 ± 2.1	1.92E-22	16	1.0 (16.1)
	B	5	$24000\,^{+3229}_{-10186}$	$0.094\,^{+0.191}_{-0.016}$	$2.7\,^{+0.8}_{-0.3}$	1.34E-25		
BSS4	A	5	8000 ± 125	2.16 ± 0.04	17.2 ± 1.5	7.06E-23	17	2.3 (9.6)
	B	5	$26000\,^{+1912}_{-13323}$	$0.089\,^{+0.304}_{-0.011}$	$3.3\,^{+0.8}_{-0.3}$	1.20E-25		
BSS5	A	3.5	6500 ± 125	2.29 ± 0.04	8.4 ± 0.8	7.90E-23	12	0.4 (19.9)
	B	5	$14000\,^{+12479}_{-5493}$	$0.237\,^{+0.376}_{-0.150}$	$1.9\,^{+2.1}_{-0.5}$	8.47E-25		
BSS7	A	3	8500 ± 125	2.90 ± 0.05	39.6 ± 1.4	1.27E-22	11	0.6 (1.4)
	B	5	$19000\,^{+8088}_{-2901}$	$0.270\,^{+0.102}_{-0.134}$	$8.6\,^{+1.2}_{-0.8}$	1.11E-24		

Name	$\log g$	T_{eff} [K]	e_T_{eff} [K]	R [$R_\odot$]	e_R [$R_\odot$]	L [$L_\odot$]	e_L [$L_\odot$]	Scaling factor	N_{fit}	χ_r^2
Single fits										
BSS6	4	6500	125	2.32	0.04	8.74	0.41	8.15E-23	11	3.4
BSS8	3	7000	125	4.19	0.07	38.17	2.05	2.66E-22	11	3.2
BSS9	3.5	7500	125	2.81	0.05	22.58	1.14	1.20E-22	11	4.2
BSS10	3	6250	125	2.91	0.05	11.67	0.54	1.28E-22	11	3.9
BSS11	4	6750	125	5.28	0.09	52.55	2.64	4.22E-22	11	1.6
BSS12	3.5	7000	125	1.97	0.03	8.66	0.43	5.85E-23	12	47.9
BSS13	3.5	6750	125	2.32	0.04	10.17	0.51	8.16E-23	11	3.2
BSS14	3	6750	125	2.38	0.04	10.63	0.48	8.54E-23	11	2.5
BSS15	3	6500	125	2.44	0.04	9.71	0.49	9.02E-23	11	3.6
BSS16	3	6750	125	1.99	0.03	7.42	0.37	6.00E-23	11	3.1
BSS17	3.5	7000	125	2.32	0.04	11.60	0.55	8.12E-23	11	4.3
BSS18	4	6500	125	2.22	0.04	8.08	0.34	7.48E-23	15	12.3
BSS19	4.5	7250	125	2.89	0.05	20.92	1.17	1.26E-22	8	13.3
BSS20	5	6500	125	2.23	0.04	8.05	0.32	7.53E-23	11	3.4
BSS21	5	6500	125	3.08	0.05	15.32	0.61	1.43E-22	11	4.9
BSS22	3.5	6250	125	3.28	0.06	14.88	0.62	1.63E-22	11	1.5
BSS23	3.5	6500	125	2.84	0.05	13.00	0.59	1.22E-22	11	3.7
BSS24	3	7250	125	2.12	0.04	11.24	0.59	6.77E-23	11	2.1
BSS25	5	6250	125	2.64	0.05	9.73	0.39	1.06E-22	15	11.7
BSS26	3	7250	125	2.28	0.04	13.06	0.67	7.89E-23	15	11.3
BSS27	4.5	6250	125	2.17	0.04	6.47	0.26	7.10E-23	11	4.3
BSS28	4	7250	125	2.23	0.04	12.57	0.68	7.54E-23	15	9.8
BSS29	4	6500	130	2.27	0.04	8.40	0.41	7.81E-23	5	125.1
BSS30	4.5	6250	125	2.45	0.04	8.35	0.34	9.08E-23	11	5.3
BSS31	5	8250	127	1.40	0.02	8.09	0.35	2.98E-23	15	9.0
BSS32	4	6250	125	2.57	0.04	9.27	0.39	9.98E-23	15	19.5
BSS33	4	6500	125	2.04	0.04	6.79	0.28	6.29E-23	15	10.9
BSS34	4	6500	125	3.80	0.07	23.42	1.01	2.19E-22	11	4.2

Table 2.   *Continued.*

Name	log g	T_{eff} [K]	e_T_{eff} [K]	R [$R_\odot$]	e_R [$R_\odot$]	L [$L_\odot$]	e_L [$L_\odot$]	Scaling factor	N_{fit}	χ_r^2
BSS35	3	6250	125	2.41	0.04	8.07	0.38	8.75E-23	11	4.4
BSS36	3.5	6500	125	2.37	0.04	9.13	0.44	8.51E-23	11	3.3
BSS37	5	6500	125	2.25	0.04	8.23	0.34	7.65E-23	11	3.6
BSS38	5	6500	125	2.68	0.05	11.70	0.48	1.09E-22	11	3.4
BSS39	3.5	6500	125	3.31	0.06	17.67	0.80	1.65E-22	11	3.9

iterations in $T_{\text{eff}}-\chi^2$ phase-plane. The double component fits of BSS2, 3, 4, 5 and 7, and single-component fits of BSS10 and BSS15 are shown in Fig. 3. The fitting parameters are mentioned in Table 2.

The H–R diagram of the BSSs detected in King 2 is shown in Fig. 4. We have shown the UV faint BSSs as blue dots, UV bright BSSs are represented as blue diamonds, and the hotter components of UV bright BSSs as filler circles. We have taken the parameters of the hotter companions detected along with the BSSs in NGC 188 from Subramaniam *et al.* 2016 and NGC 2682 from Sindhu *et al.* (2019), Jadhav *et al.* (2019) and Sindhu *et al.* (in prep.). They are plotted in the figure as orange cross and triangles respectively. The parameters of the EHB stars in NGC 1851 are taken from Singh *et al.* (2020) and are shown as orange stars. The PARSEC[4] isochrone of log age = 9.7 is over-plotted and shown in black (Bressan *et al.* 2012), along with the WD cooling curves[5] (thick grey curves, Tremblay & Bergeron 2009) and BaSTI[6] zero age HB (ZAHB; dashed black curve; Hidalgo *et al.* 2018).

4. Results and discussion

BSS and their companions in literature

The BSSs have T_{eff} range of 5750 to 8500 K and radii of 1.4 to 5.21$R_\odot$. By comparison to isochrones, they have mass in the range of 1.2 to 1.9$M_\odot$, the brightest BSS being 3 mag brighter than the MSTO. Majority of BSSs in King 2 have T_{eff} similar to the older NGC 188 (6100–6800 K; Gosnell *et al.* 2015), but are cooler than NGC 2682 (6250–9000 K; Sindhu *et al.* in prep.), which is expected due to its slightly younger age. The BSSs in NGC 188 (Geller & Mathieu 2011; Gosnell *et al.* 2014; Subramaniam *et al.* 2016) and NGC 2682

(Sindhu *et al.* 2019) are known to have evolved companions. The companions were classified as WD, ELM WDs, post-AGB/HB according to their luminosity and temperature.

BSS2-A, BSS3-A and BSS7-A lie above/on the ZAHB in Fig. 3. There is a degeneracy in this region of the H–R diagram where one could find both massive BSS as well as ZAHB stars. Stars in these two evolutionary phases will have different masses (HB mass < MSTO; BSS mass > MSTO), that could be used to lift the degeneracy. Bond and Perry (1971) measured the masses of stars in this region of the NGC 2682 CMD and determined that they are indeed high mass BSSs. One star is found in this region of the NGC 188 CMD and it is classified as a BHB (Rani *et al.* 2021), this star is significantly brighter than the rest of the BSSs. In the case of King 2, the BSSs show a continuous distribution up to the brightest BSS, hence BSS2-A/BSS3-A are most likely normal BSSs. However, their mass estimations (via log g measurements or asteroseismology) are required before confirming their evolutionary status.

What are the hotter companions?

The hotter companions in UV bright BSSs have T_{eff} of 14000 to 26000 K (spectral type B) and radii of 0.09 to 0.27$R_\odot$. Figure 3 shows the density distributions of the best 100 fits for the hotter companions. Figure 3 also shows the location of various companions to BSS in NGC 188 and NGC 2682, and EHB stars in NGC 1851, one of which has a BSS as its companion (Singh *et al.* 2020).

The hotter companion to BSSs in NGC 2682 are all fainter and near the WD cooling curves. While those for NGC 1851 and NGC 188 lie closer to the ZAHB region. In King 2, the limiting magnitude of UVIT observations is 23 and 22 mag in F148W and N219M, respectively. According to WD cooling models (corrected for distance and extinction; Tremblay & Bergeron 2009), only WDs younger than 0.7 and 16

---

[4] http://stev.oapd.inaf.it/cgi-bin/cmd

[5] www.astro.umontreal.ca/~bergeron/CoolingModels/

[6] http://basti-iac.oa-abruzzo.inaf.it/isocs.html

Table 3. Coordinates, Gaia EDR3 source IDs, flux and flux errors of the stars in all used filters. All flux are given in erg s^{-1} cm^{-2} Å^{-1}. GALEX, Gaia (EDR3), Pan-Starrs (PS1) and 2MASS photometry is taken from archives. CAHA photometry is taken from A90.

| Name	R.A. (J2016)	Dec. (J2016)	Gaia EDR3 source_id	UVIT.F148W±err	UVIT.N219M±err	GALEX.NUV±err	CAHA.U±err	CAHA.B±err
BSS1	12.735411	58.185675	4244168871060018688	1.87e-16±2.18e-17	–	2.74e-16±6.08e-17	8.05e-16±1.29e-17	1.11e-15±1.45e-17
BSS2	12.851678	58.152155	4244150660399931520	1.08e-15±5.07e-17	4.67e-16±3.57e-17	6.86e-16±6.07e-17	1.21e-15±1.94e-17	1.68e-15±2.20e-17
BSS3	12.748154	58.207693	4244183989344848480	1.57e-16±2.16e-17	–	2.51e-16±4.47e-17	7.21e-16±9.45e-18	9.75e-16±9.03e-18
BSS4	12.741835	58.196669	4244183645747755328	2.03e-16±2.17e-17	1.07e-16±2.9e-17	2.30e-16±4.14e-17	–	–
BSS5	12.676827	58.114184	4244162342710159072		4.98e-17±1.53e-17	4.93e-17±3.16e-17	–	–
BSS6	12.852115	58.202338	4244156845151168768		–	–	–	–
BSS7	12.497494	58.135206	4250740171009147968	6.42e-16±3.65e-17	3.96e-16±3.82e-17	4.86e-16±4.40e-17	–	–
BSS8	12.475572	58.232940	4251684333610105568	1.96e-16±2.09e-17	1.31e-16±2.8e-17	–	–	–
BSS9	12.562694	58.306732	4251703618077107392	7.94e-17±1.43e-17	–	1.76e-16±4.34e-17	–	–
BSS10	12.951969	58.156780	4244142070464175904		5.57e-17±1.51e-17	–	–	–
BSS11	12.601162	58.118577	4243233942584115744		1.14e-16±2.18e-17	1.23e-16±2.83e-17	3.00e-16±1.16e-17	4.42e-16±1.49e-17
BSS12	12.718310	58.184925	4244169171608168480			8.45e-17±3.9e-17	–	–
BSS13	12.668926	58.042374	4243218094051171968			3.74e-17±1.55e-17	–	–
BSS14	12.677840	58.058054	4243222260274137440			–	–	–
BSS15	12.630396	58.055428	4243225696247103744			3.68e-17±1.72e-17	–	–
BSS16	12.578670	58.094139	42432874557099008			–	–	–
BSS17	12.637498	58.089431	424323016301297792			6.69e-17±3.16e-17	2.52e-16±5.75e-18	3.74e-16±7.79e-18
BSS18	12.729170	58.183177	424416921465758976			–	–	–
BSS19	12.585603	58.116081	424323291174262400			1.13e-15±6.10e-17	–	–
BSS20	12.703872	58.117638	424416268630796672			6.26e-17±2.11e-17	–	–
BSS21	12.916705	58.156035	424414928600979712			–	–	–
BSS22	12.792388	58.127478	424416436124233344			4.66e-17±2.28e-17	–	–
BSS23	12.755911	58.107444	424416096832121088			–	–	–
BSS24	12.600595	58.148060	424417265062966656			–	–	–
BSS25	12.792363	58.189219	424418188471143040			–	2.71e-16±3.56e-18	3.99e-16±3.69e-18
BSS26	12.744375	58.209324	424418394634254720			3.23e-16±5.68e-17	5.17e-16±8.32e-18	7.68e-16±1.01e-17
BSS27	12.669486	58.259244	424419395366848640			–	–	–
BSS28	12.751046	58.197227	424418360269944320			1.73e-16±4.38e-17	4.46e-16±0.0e+00	6.75e-16±0.e+00
BSS29	12.651172	58.264862	424419601519284096			3.58e-16±4.71e-17	–	–
BSS30	12.944214	58.230622	424421456951191040			–	–	–
BSS31	12.741104	58.182103	4244168871060023168			–	3.32e-16±5.35e-18	4.67e-16±6.12e-18
BSS32	12.736065	58.182505	4244168871060023040			–	2.64e-16±6.02e-18	4.07e-16±8.46e-18
BSS33	12.759065	58.182083	4244168871060024704			7.26e-17±3.01e-17	2.12e-16±3.40e-18	3.14e-16±4.12e-18
BSS34	12.516954	58.129105	4250739440813050784			–	–	–
BSS35	12.507227	58.180810	4250741888996001024			–	–	–
BSS36	12.551578	58.191653	425168094064999808			8.47e-17±2.75e-17	–	–
BSS37	12.533187	58.207971	425168162784475008			–	–	–
BSS38	12.530339	58.248740	425168609461065344			–	–	–
BSS39	12.532937	58.265730	425168918970688688			–	–	–

Table 3. *Continued.*

| Name	CAHA.V±err	CAHA.R±err	GAIA3.Gbp±err	GAIA3.G±err	GAIA3.Grp±err	PS1.r±err	PS1.g±err	PS1.i±err
BSS1	1.04e-15±9.6e-18	7.48e-16±1.56e-17	1.05e-15±3.77e-18	9.17e-16±2.42e-18	6.33e-16±2.98e-18	8.98e-16±2.18e-18	1.17e-15±6.58e-18	6.57e-16±3.91e-18
BSS2	—	—	3.31e-15±9.33e-18	2.73e-15±7.e-18	1.76e-15±6.5e-18	2.63e-15±4.42e-18	3.73e-15±3.04e-18	1.81e-15±5.46e-18
BSS3	1.66e-15±1.53e-17	1.17e-15±1.54e-17	1.74e-15±1.18e-17	1.44e-15±3.74e-18	1.14e-15±8.38e-18	1.47e-15±1.16e-17	1.82e-15±6.67e-18	1.10e-15±1.27e-17
BSS4	9.37e-16±0.e+00	6.64e-16±6.14e-18	9.13e-16±4.15e-18	7.77e-16±2.13e-18	5.48e-16±3.35e-18	7.69e-16±4.1e-18	9.92e-16±5.18e-18	5.56e-16±3.92e-18
BSS5	—	—	3.95e-16±8.03e-18	3.82e-16±2.38e-18	2.96e-16±5.61e-18	4.26e-16±1.86e-18	4.86e-16±1.02e-17	3.60e-16±9.59e-19
BSS6	—	—	4.35e-16±2.74e-18	4.31e-16±1.12e-18	3.47e-16±1.73e-18	4.34e-16±1.30e-18	4.47e-16±6.11e-19	3.57e-16±1.66e-18
BSS7	—	—	2.22e-15±6.52e-18	1.81e-15±4.63e-18	1.15e-15±4.43e-18	1.75e-15±2.87e-18	2.52e-15±4.96e-18	1.19e-15±1.7e-18
BSS8	—	—	2.17e-15±9.38e-18	1.78e-15±5.63e-18	1.44e-15±6.71e-18	1.94e-15±4.52e-18	2.38e-15±2.27e-17	1.51e-15±6.08e-18
BSS9	—	—	1.24e-15±3.85e-18	1.10e-15±2.83e-18	7.85e-16±2.92e-18	1.09e-15±2.63e-18	1.36e-15±5.10e-18	8.17e-16±1.91e-18
BSS10	—	—	5.81e-16±2.82e-18	5.97e-16±1.54e-18	4.86e-16±2.03e-18	5.96e-16±1.29e-18	5.98e-16±1.66e-18	5.06e-16±1.76e-18
BSS11	—	—	2.71e-15±8.32e-18	2.54e-15±6.92e-18	2.06e-15±7.59e-18	2.62e-15±3.41e-18	2.79e-15±1.59e-17	2.10e-15±4.01e-18
BSS12	4.57e-16±8.49e-18	3.3e-16±8.7e-18	5.41e-16±5.55e-18	4.12e-16±1.11e-18	3.8e-16±5.22e-18	4.71e-16±2.73e-18	5.4e-16±1.11e-17	3.12e-16±3.80e-19
BSS13	—	—	5.22e-16±2.54e-18	5.1e-16±1.32e-18	3.91e-16±1.81e-18	5.17e-16±1.98e-18	5.58e-16±1.13e-18	4.1e-16±2.38e-18
BSS14	—	—	5.58e-16±2.88e-18	5.40e-16±1.4e-18	4.18e-16±1.93e-18	5.41e-16±1.41e-18	5.94e-16±3.12e-18	4.32e-16±1.15e-18
BSS15	—	—	5.08e-16±2.38e-18	4.93e-16±1.28e-18	3.91e-16±1.87e-18	4.93e-16±4.97e-18	5.24e-16±2.41e-18	3.99e-16±9.95e-19
BSS16	—	—	3.89e-16±2.6e-18	3.80e-16±1.00e-18	2.93e-16±1.67e-18	3.82e-16±1.94e-18	4.24e-16±1.89e-18	3.04e-16±1.66e-18
BSS17	—	—	6.09e-16±2.68e-18	5.79e-16±1.49e-18	4.37e-16±1.76e-18	5.8e-16±1.76e-18	6.61e-16±2.81e-18	4.55e-16±2.08e-18
BSS18	4.32e-16±4.e-18	3.48e-16±7.25e-18	4.26e-16±2.36e-18	4.14e-16±1.11e-18	3.21e-16±1.65e-18	4.14e-16±1.49e-18	4.59e-16±1.32e-18	3.29e-16±2.25e-18
BSS19	—	—	1.11e-15±1.67e-17	9.60e-16±2.47e-18	7.52e-16±5.66e-18	1.11e-15±6.75e-17	1.09e-15±4.76e-18	7.48e-16±3.34e-18
BSS20	—	—	3.91e-16±2.34e-18	3.95e-16±1.03e-18	3.22e-16±1.65e-18	3.92e-16±1.55e-18	4.03e-16±1.12e-18	3.34e-16±1.13e-18
BSS21	—	—	7.4e-16±3.48e-18	7.54e-16±1.94e-18	6.12e-16±2.69e-18	7.54e-16±2.82e-18	7.69e-16±1.61e-18	6.36e-16±1.77e-18
BSS22	—	—	7.48e-16±3.48e-18	6.97e-16±1.83e-18	6.42e-16±2.76e-18	7.62e-16±2.52e-18	7.44e-16±1.84e-18	6.41e-16±2.33e-18
BSS23	—	—	6.58e-16±3.64e-18	6.49e-16±1.68e-18	5.25e-16±2.48e-18	6.58e-16±3.49e-18	6.84e-16±1.84e-18	5.47e-16±1.15e-18
BSS24	—	—	6.26e-16±2.97e-18	5.66e-16±1.46e-18	4.01e-16±1.65e-18	5.70e-16±1.94e-18	6.87e-16±3.e-18	4.21e-16±1.53e-18
BSS25	5.25e-16±0.e+00	4.42e-16±4.09e-18	4.83e-16±2.45e-18	4.99e-16±1.29e-18	4.11e-16±1.73e-18	4.99e-16±1.66e-18	4.92e-16±2.24e-18	4.20e-16±1.15e-18
BSS26	7.72e-16±7.15e-18	5.47e-16±1.14e-17	7.67e-16±3.92e-18	6.56e-16±1.7e-18	4.77e-16±2.45e-18	6.63e-16±1.22e-18	8.35e-16±3.78e-18	4.83e-16±2.19e-18
BSS27	—	—	3.13e-16±2.65e-18	3.22e-16±8.48e-19	2.68e-16±1.53e-18	3.21e-16±1.05e-18	3.14e-16±1.08e-18	2.76e-16±1.51e-18
BSS28	7.04e-16±0.e+00	5.13e-16±0.e+00	7.09e-16±3.49e-18	6.11e-16±1.58e-18	4.58e-16±3.21e-18	6.28e-16±3.32e-18	7.66e-16±6.66e-18	4.64e-16±4.53e-18
BSS29	—	—	4.93e-16±1.33e-17	3.24e-16±1.01e-18	3.96e-16±5.41e-18	—	—	3.53e-16±1.56e-18
BSS30	—	—	3.99e-16±2.37e-18	4.11e-16±1.07e-18	3.42e-16±1.91e-18	4.11e-16±1.73e-18	4.04e-16±1.69e-18	3.53e-16±2.26e-18
BSS31	4.40e-16±4.07e-18	3.03e-16±6.31e-18	4.42e-16±1.99e-18	3.77e-16±9.87e-19	2.48e-16±1.33e-18	3.69e-16±1.07e-18	5.e-16±2.37e-18	2.6e-16±7.87e-19
BSS32	5.01e-16±4.64e-18	4.19e-16±8.71e-18	4.91e-16±6.23e-18	4.95e-16±2.30e-18	3.89e-16±4.94e-18	5.35e-16±3.38e-18	4.50e-16±3.41e-18	3.73e-16±1.09e-17
BSS33	3.7e-16±3.42e-18	2.92e-16±6.08e-18	3.58e-16±1.94e-18	3.44e-16±9.05e-19	2.7e-16±1.42e-18	3.48e-16±1.96e-18	3.74e-16±1.76e-18	2.77e-16±1.17e-18
BSS34	—	—	1.14e-15±4.32e-18	1.16e-15±2.97e-18	9.36e-16±3.78e-18	1.16e-15±2.23e-18	1.2e-15±4.82e-18	9.64e-16±3.07e-18
BSS35	—	—	4.02e-16±2.9e-18	4.09e-16±1.07e-18	3.32e-16±1.81e-18	4.04e-16±2.08e-18	4.21e-16±2.32e-18	3.41e-16±1.22e-18
BSS36	—	—	4.58e-16±2.33e-18	4.61e-16±1.19e-18	3.65e-16±1.9e-18	4.63e-16±1.08e-18	4.76e-16±1.54e-18	3.74e-16±1.76e-18
BSS37	—	—	3.98e-16±2.75e-18	4.02e-16±1.04e-18	3.25e-16±1.65e-18	4.04e-16±2.1e-18	4.04e-16±2.03e-18	3.36e-16±3.62e-18
BSS38	—	—	5.62e-16±2.29e-18	5.72e-16±1.48e-18	4.63e-16±2.08e-18	5.77e-16±2.91e-18	5.80e-16±2.53e-18	4.79e-16±2.68e-18
BSS39	—	—	8.86e-16±3.28e-18	8.86e-16±2.27e-18	7.11e-16±2.90e-18	9.05e-16±5.27e-18	9.20e-16±2.39e-18	7.36e-16±1.62e-18

Table 3. *Continued.*

Name	PS1.z±err	PS1.y±err	2MASS.J±err	2MASS.H±err	2MASS.Ks±err
BSS1	5.25e-16±1.08e-18	4.74e-16±2.72e-18	2.62e-16±2.54e-17	1.13e-16±1.34e-17	5.08e-17±4.92e-18
BSS2	1.39e-15±4.31e-18	1.22e-15±3.58e-18	6.45e-16±1.90e-17	2.62e-16±9.67e-18	1.11e-16±5.71e-18
BSS3	9.14e-16±1.53e-17	8.26e-16±5.47e-18	5.06e-16±2.24e-17	2.38e-16±1.18e-17	9.34e-17±5.51e-18
BSS4	4.4e-16±3.34e-18	3.93e-16±3.24e-18	2.49e-16±2.09e-17	1.23e-16±1.08e-17	5.51e-17±4.98e-18
BSS5	2.43e-16±5.71e-18	2.58e-16±1.69e-18	1.72e-16±8.39e-18	8.52e-17±8.16e-18	3.49e-17±4.5e-18
BSS6	2.99e-16±9.55e-19	2.69e-16±2.31e-18	1.68e-16±8.98e-18	8.63e-17±7.15e-18	2.51e-17±4.62e-18
BSS7	9.12e-16±3.76e-18	8.00e-16±3.15e-18	4.13e-16±1.10e-17	1.62e-16±8.08e-18	7.57e-17±4.60e-18
BSS8	1.18e-15±9.73e-18	1.04e-15±7.33e-18	6.38e-16±1.82e-17	2.81e-16±1.14e-17	1.35e-16±6.98e-18
BSS9	6.41e-16±1.70e-18	5.95e-16±4.39e-18	3.28e-16±1.18e-17	1.22e-16±7.77e-18	6.14e-17±4.64e-18
BSS10	4.28e-16±1.07e-18	3.83e-16±2.33e-18	2.35e-16±9.74e-18	1.1e-16±7.49e-18	4.01e-17±4.43e-18
BSS11	1.71e-15±9.50e-19	1.49e-15±4.28e-18	8.75e-16±2.74e-17	4.44e-16±1.55e-17	1.79e-16±6.59e-18
BSS12	2.62e-16±7.86e-18	2.29e-16±3.82e-18	–	–	–
BSS13	3.31e-16±1.17e-18	2.94e-16±1.54e-18	1.90e-16±8.77e-18	7.19e-17±8.28e-18	3.57e-17±4.53e-18
BSS14	3.52e-16±1.72e-18	3.15e-16±9.87e-19	1.81e-16±9.68e-18	9.1e-17±8.05e-18	3.39e-17±4.47e-18
BSS15	3.27e-16±8.77e-19	3.e-16±2.43e-18	1.76e-16±1.34e-17	8.93e-17±1.00e-17	3.82e-17±4.71e-18
BSS16	2.48e-16±1.38e-18	2.17e-16±1.34e-18	1.22e-16±8.34e-18	4.58e-17±7.26e-18	3.06e-17±4.23e-18
BSS17	3.69e-16±9.43e-19	3.35e-16±1.67e-18	1.95e-16±9.35e-18	7.14e-17±8.22e-18	2.53e-17±4.2e-18
BSS18	2.72e-16±1.06e-18	2.48e-16±4.72e-18	1.40e-16±1.03e-17	7.21e-17±7.51e-18	2.63e-17±4.23e-18
BSS19	6.05e-16±2.66e-18	5.45e-16±5.40e-18	–	–	–
BSS20	2.76e-16±1.32e-18	2.49e-16±1.19e-18	1.40e-16±8.54e-18	6.93e-17±7.35e-18	3.35e-17±4.38e-18
BSS21	5.32e-16±2.70e-18	4.8e-16±2.17e-18	2.52e-16±1.02e-17	1.42e-16±7.47e-18	5.78e-17±4.63e-18
BSS22	5.30e-16±3.77e-18	4.75e-16±3.28e-18	2.99e-16±1.26e-17	1.65e-16±8.21e-18	6.69e-17±4.81e-18
BSS23	4.51e-16±1.68e-18	4.12e-16±1.62e-18	2.41e-16±1.84e-17	1.08e-16±1.24e-17	3.85e-17±4.39e-18
BSS24	3.34e-16±1.49e-18	2.97e-16±1.90e-18	1.63e-16±1.14e-17	8.01e-17±8.78e-18	3.33e-17±4.36e-18
BSS25	3.57e-16±1.07e-18	3.24e-16±3.41e-18	1.80e-16±9.14e-18	9.28e-17±7.43e-18	3.86e-17±4.62e-18
BSS26	3.92e-16±2.16e-18	3.78e-16±2.60e-18	2.06e-16±2.72e-17	1.02e-16±1.42e-17	2.97e-16±0.e+00
BSS27	2.34e-16±8.07e-19	2.15e-16±2.34e-18	1.29e-16±9.73e-18	5.7e-17±8.24e-18	2.50e-17±4.08e-18
BSS28	3.72e-16±2.29e-18	3.35e-16±2.27e-18	1.84e-16±1.77e-17	8.e-17±1.08e-17	3.44e-17±5.70e-18
BSS29	2.83e-16±3.36e-19	–	–	–	–
BSS30	2.97e-16±2.38e-18	2.73e-16±2.7e-18	1.75e-16±1.01e-17	7.47e-17±7.36e-18	4.95e-17±4.47e-18
BSS31	1.97e-16±8.58e-19	1.76e-16±1.28e-18	8.13e-17±7.64e-18	5.44e-17±0.e+00	1.57e-17±0.e+00
BSS32	3.29e-16±7.91e-18	2.68e-16±6.06e-18	1.60e-16±1.2e-17	8.60e-17±1.11e-17	3.44e-17±4.47e-18
BSS33	2.3e-16±9.57e-19	2.1e-16±2.92e-18	1.16e-16±1.36e-17	5.84e-17±9.30e-18	3.00e-17±4.79e-18
BSS34	8.05e-16±1.36e-18	7.30e-16±2.53e-18	4.40e-16±1.3e-17	2.05e-16±8.11e-18	9.78e-17±4.96e-18
BSS35	2.88e-16±9.61e-19	2.6e-16±3.76e-18	1.80e-16±9.80e-18	7.33e-17±6.75e-18	3.7e-17±4.26e-18
BSS36	3.17e-16±4.78e-19	2.78e-16±3.62e-18	1.68e-16±9.89e-18	8.51e-17±6.97e-18	3.27e-17±4.31e-18
BSS37	2.8e-16±2.77e-18	2.51e-16±2.45e-18	1.60e-16±9.29e-18	7.96e-17±6.89e-18	3.00e-17±4.59e-18
BSS38	3.99e-16±2.09e-18	3.57e-16±1.09e-18	2.24e-16±1.07e-17	1.07e-16±7.31e-18	4.86e-17±4.70e-18
BSS39	6.08e-16±1.66e-18	5.54e-16±2.85e-18	3.34e-16±1.23e-17	1.46e-16±8.77e-18	6.36e-17±4.69e-18
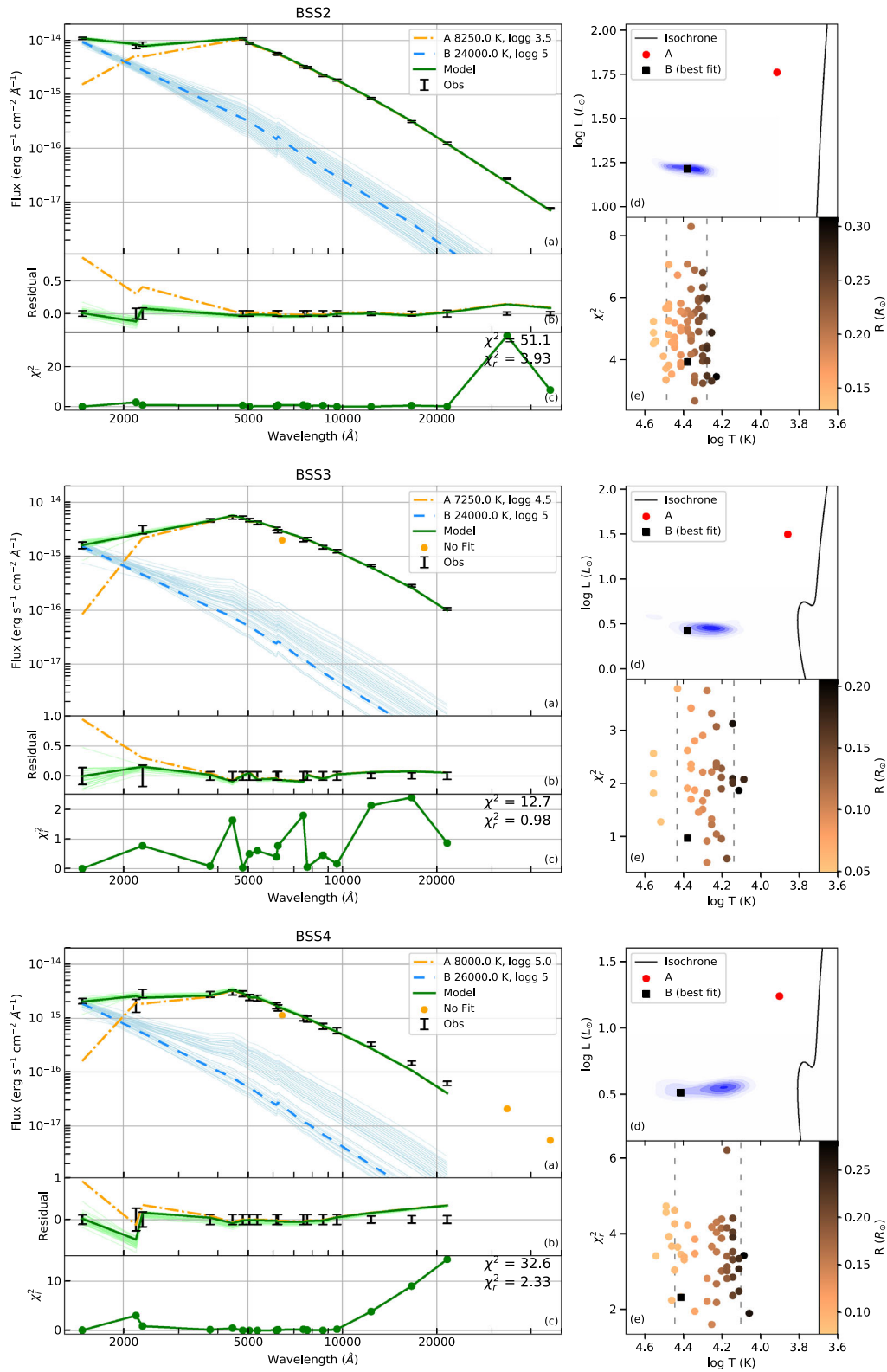
Figure 3. The descriptions of double component fits are same as Fig. 2. The single component fits of BSS10 and BSS15 are shown as an example with model fit (blue curve), fitted data points (red points) with 1σ and 3σ errors as solid and dashed lines. The theoretical spectra (in grey) is added for reference. The observed (reddening affected) SED is shown in grey below the corrected data-points. The title mentions the T_{eff}, $\log g$, metallicity and A_V of the model fit.
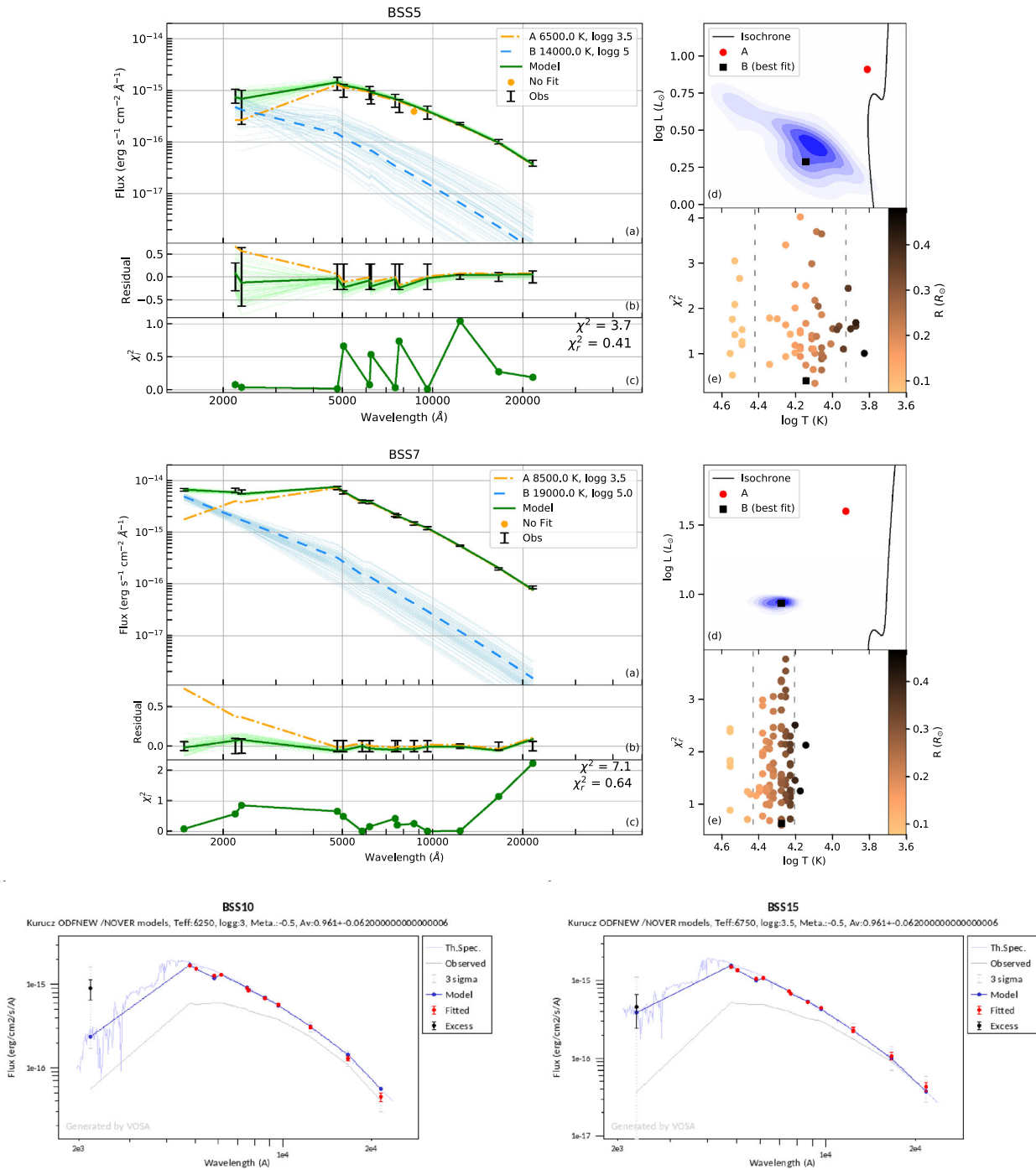
Figure 3. *Continued.*

Myr old would be detectable. As seen in Fig. 4, the hotter companions are well above the WD cooling curves, and these are not WDs.

The hotter companions are likely to be hot HB stars which are also known as EHB stars or sdB stars, as inferred from their T_{eff}, radii and luminosity. These are core-helium burning stars with T_{eff} in the range of 20,000–40,000 K and are compact (0.15–$0.35 R_{\odot}$; Heber 2016; Sahoo *et al.* 2020). As these stars are hot and not as small as WDs, they appear bright in the UV. These stars are thought to contribute to the UV upturn seen in elliptical or in early-type galaxies (Brown *et al.* 1997). The sdB stars have very thin hydrogen envelope and are
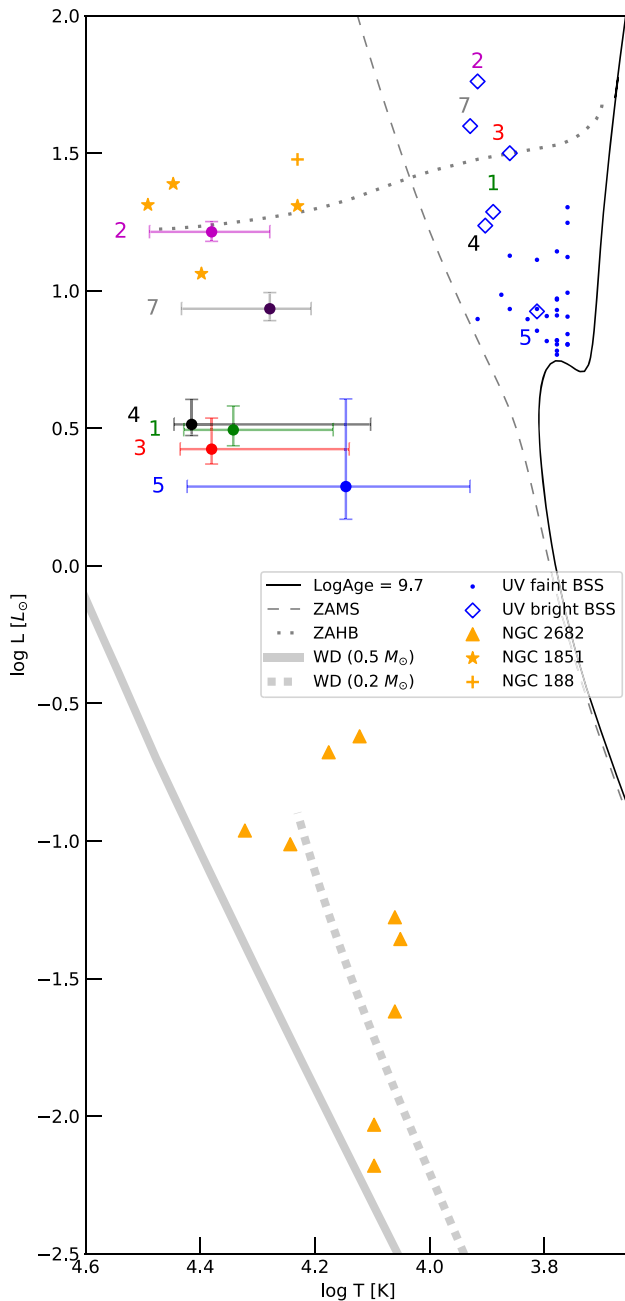
Figure 4. H–R diagram of locations of components of binaries in King 2, NGC 2682 (Sindhu *et al.* 2019; Jadhav *et al.* (2019); Sindhu *et al.* in prep.), NGC 188 (Subramaniam *et al.* 2016) and EHB stars in NGC 1851 (Singh *et al.* 2020). In King 2, the UV faint BSS (blue dots), UV bright BSS (blue diamonds with their ID) and hotter components in BSSs (coloured filled circles with numbers and error bars) are shown. Hotter components in NGC 2682 and NGC 188 are shown as orange triangles and cross. EHB stars in NGC 1851 are shown as stars. The PARSEC isochrone (black curve), PARSEC zero age MS (dashed grey line), WD cooling curves (thick grey curves) and BaSTI ZAHB (dotted grey curve) are shown for reference.

thought to be the stripped core of a red giant star (Heber 2016). Maxted *et al.* (2001) found a good fraction of the sdB stars in detached, but short period binary systems. sdB stars are thought to provide important clues to common envelope evolution in tight binaries.

BSS2-B lies on the blue end of ZAHB and very similar to the EHBs in the outskirts of GC NGC 1851. Similarly, hot and bright post-AGB/HB candidate was found as a companion to a BSS in NGC 188 (Subramaniam *et al.* 2016). Hence, BSS2-B could be an EHB star. BSS7-B is near a known EHB from NGC 1851 and is slightly fainter than ZAHB, hence, it is likely to be an EHB. BSS5-B lies slightly above the WDs. Hence, it can be a very young He-WD (Panei *et al.* 2007) or an sdB star. Rest of the King 2 BSS companions are slightly fainter than the ZAHB, and they are likely sdBs.

Formation pathways of BSSs and EHBs/sdBs

BSS formation mechanism involves mass gain while the EHB/sdB formation involves the stripping of the envelope of a post-MS star. The detection of EHB/sdBs confirms 'binary mass transfer' as the formation mechanism for BSS1 to BSS5 and BSS7. As the cooler companions are BSSs that are supposed to have gained mass, we can infer that the detected EHBs/sdBs have transferred mass to the BSSs companions. Therefore, the BSS+EHB/sdB systems in King 2 illustrate stars on both sides of the mass exchange. We see a range in their temperature and luminosity, suggesting a diversity among the hotter companions.

The lifespan of sdB stars is expected to be between 100 to 200 Myr (Bloemen *et al.* 2014; Schindler *et al.* 2015 and references therein), after which they descend the WD cooling curve. When the current BSS expands, the mass transfer is expected to start again due to the short orbit, which already allowed the previous instance of mass transfer. The system can begin stable/unstable mass transfer and become a WD+WD system. Alternatively, it can merge through a common-envelope phase and become a massive WD. The exact evolution will depend on then orbital parameters, mass transfer efficiency and mass loss.

King 2 is one of the oldest OC, lies in the outskirts of the galactic disk. It is metal-poor compared to the Galactic disc OCs. The environment is quite similar to outskirts of GCs, which are also metal-poor, old and

of comparable density. While most of the BSSs in GCs lie in core and are formed via mergers (Chatterjee *et al.* 2013), BSSs in outskirts of GCs can form through mass transfer as seen in EHB-4 of NGC 1851 (Singh *et al.* 2020). Our study suggests that the at least 15% of the BSSs in King 2 are formed via mass transfer pathway of formation.

We have seen sdB companions to BSSs in NGC 188 and NGC 1851 (both are older systems), however none in NGC 2682 (which is younger). NGC 6791 of slightly younger age also has sdB stars (Kaluzny & Udalski 1992; Reed *et al.* 2012). This might suggest that there is an upper age limit of ~ 5 Gyr for the formation of sdB stars in OCs.

5. Conclusions and summary

- The old OC King 2 has a large population (39) of BSSs, spreading up to 3 mag brighter than the MSTO. We constructed SEDs of all the BSS using UV to IR data. The BSSs have $T_{\rm eff}$ in the range of 5750–8250 K, luminosity in the range of 5.6–57.5$L_\odot$ and mass in the range of 1.2–1.9$M_\odot$.
- Six of the UV bright BSS showed excess UV flux and were successfully fitted with double component SEDs. The hotter components have $T_{\rm eff}$ of 14000–26000 K and $R/R_\odot$ of 0.09–0.27, suggesting a range of properties. Two of the hotter companions to the BSS are likely EHB stars, while four are likely sdB stars.
- EHB/sdB companions imply that these 6 (out of 39) BSSs have formed via binary mass transfer. The SED fits show that sdB stars can be created in old OCs such as King 2 (similar to old OC NGC 188 and GC NGC 1851).

Spectroscopic time series and radial velocity variations can uncover the binary nature as well as properties of these systems and help in estimating the log g and mass of these stars. The mass and orbital estimations will expand our knowledge of BSS, EHB and sdB formation scenarios.

Acknowledgements

References

Ahumada J. A., Lapasset E. 2007, A&A, 463, 789

Andrae R., Schulze-Hartung T., Melchior P. 2010, arXiv e-prints, arXiv:1012.3754

Aparicio A., Bertelli G., Chiosi C., Garcia-Pelayo J. M. 1990, A&A, 240, 262

Bayo A., Rodrigo C., Barrado Y., Navascués D. *et al.* 2008, A&A, 492, 277

Bianchi L., GALEX Team 2000, Memorie della Società Astronomia Italiana, 71, 1123

Bloemen S., Hu H., Aerts C. *et al.* 2014, A&A, 569, A123

Bond H. E., Perry C. L. 1971, Pub. Astron. Soc. Pac., 83, 638

Bressan A., Marigo P., Girardi L., Salasnich B., Dal Cero C., Rubele S., Nanni A. 2012, MNRAS, 427, 127

Brown T. M., Ferguson H. C., Davidsen A. F., Dorman B. 1997, ApJ, 482, 685

Cantat-Gaudin T., Jordi C., Vallenari *et al.* 2018, A&A, 618, A93

Castelli F., Gratton R. G., Kurucz R. L. 1997, A&A, 318, 841

Chambers K. C., Magnier E. A., Metcalfe N. *et al.* 2016, arXiv e-prints, arXiv:1612.05560

Chatterjee S., Rasio F. A., Sills A., Glebbeek E. 2013, ApJ, 777, 106

Dias W. S., Alessi B. S., Moitinho A., Lépine J. R. D. 2002, A&A, 389, 871

Fitzpatrick E. L. 1999, Pub. Astron. Soc. Pac., 111, 63

Friel E. D., Janes K. A., Tavarez M., Scott J., Katsani R., Lotz J., Hong L., Miller N. 2002, AJ, 124, 2693

Gaia Collaboration, Brown A. G. A., Vallenari A. *et al.* 2018, A&A, 616, A1

Gaia Collaboration, Brown A. G. A., Vallenari A. *et al.* 2020, arXiv e-prints, arXiv:2012.01533

Geller A. M., Mathieu R. D. 2011, Nature, 478, 356

Gosnell N. M., Mathieu R. D., Geller A. M., Sills A., Leigh N., Knigge C. 2014, ApJL, 783, L8

Gosnell N. M., Mathieu R. D., Geller A. M., Sills A., Leigh N., Knigge C. 2015, ApJ, 814, 163

Han Z., Podsiadlowski P., Maxted P. F. L., Marsh T. R., Ivanova N. 2002, MNRAS, 336, 449

Heber U. 2016, Pub. Astron. Soc. Pac., 128, 082001

Heggie D. C. 1975, MNRAS, 173, 729

Hidalgo S. L., Pietrinferni A., Cassisi S. *et al.* 2018, ApJ, 856, 125

Indebetouw R., Mathis J. S., Babler B. L. *et al.* 2005, ApJ, 619, 931

Jadhav V. V., Sindhu N., Subramaniam A. 2019, ApJ, 886, 13

Jadhav V. V., Pennock C. M., Subramaniam A., Sagar R., Nayak P. K. 2021, MNRAS, 503, 236

Kaluzny J. 1989, Acta Astron., 39, 13

Kaluzny J., Udalski A. 1992, Acta Astron., 42, 29

Kozai Y. 1962, AJ, 67, 591

Kumar A., Ghosh S. K., Hutchings J. *et al.* 2012, SPIE, 8443, 84431N

Leiner E., Mathieu R. D., Vanderburg A., Gosnell N. M., Smith J. C. 2019, ApJ, 881, 47

Marsh T. R., Dhillon V. S., Duck S. R. 1995, MNRAS, 275, 828

Maxted P. F. L., Heber U., Marsh T. R., North R. C. 2001, MNRAS, 326, 1391

Panei J. A., Althaus L. G., Chen X., Han Z. 2007, MNRAS, 382, 779

Postma J. E., Leahy D. 2017, Pub. Astron. Soc. Pac., 129, 115002

Rani S., Subramaniam A., Pandey S., Sahu S., Mondal C., Pandey G. 2021, J. Astrophys. Astr., 42, https://doi.org/10.1007/s12036-020-09683-2

Reed M. D., Baran A., Tensen R. H., Telting J., O'Toole S. J. 2012, MNRAS, 427, 1245

Rucinski S. M. 1998, AJ, 116, 2998

Sahoo S. K., Baran A. S., Heber U. *et al.* 2020, MNRAS, 495, 2844

Sahu S., Subramaniam A., Simunovic M. *et al.* 2019, ApJ, 876, 34

Schindler J.-T., Green E. M., Arnett W. D. 2015, ApJ, 806, 178

Sindhu N., Subramaniam A., Jadhav V. V. *et al.* 2019, ApJ, 882, 43

Singh G., Sahu S., Subramaniam A., Yadav R. K. S. 2020, ApJ, 905, 44

Skrutskie M. F., Cutri R. M., Stiening R. *et al.* 2006, AJ, 131, 1163

Subramaniam A., Sindhu N., Tandon S. N. *et al.* 2016, ApJL, 833, L27

Subramaniam A., Pandey S., Jadhav V. V., Sahu S. 2020, J. Astrophys. Astr., 41, 45

Tadross A. L. 2001, New Astronomy, 6, 293

Tandon S. N., Hutchings J. B., Ghosh S. K. *et al.* 2017, J. Astrophys. Astr., 38, 28

Taylor M. B. 2005, Astronomical Data Analysis Software and Systems XIV, 347, 29

Tody D. 1993, Astronomical Data Analysis Software and Systems II, 52, 173

Tremblay P.-E., Bergeron P. 2009, ApJ, 696, 1755

Warren S. R., Cole A. A. 2009, MNRAS, 393, 272

Wright E. L., Eisenhardt P. R. M., Mainzer *et al.* 2010, AJ, 140, 1868